Journal of Solid State Chemistry **163**, 385–389 (2002)
doi:10.1006/jssc.2001.9374, available online at http://www.idealibrary.com on IDEAL®

Synthesis, Structure, and Superconductivity in $Be_{1.09}B_3$

Julia Y. Chan[1] and Frank R. Fronczek

Department of Chemistry, Louisiana State University, Baton Rouge, Louisiana 70803

and

D. P. Young, J. F. DiTusa, and P. W. Adams

Department of Physics and Astronomy, Louisiana State University, Baton Rouge, Louisiana 70803

Received June 18, 2001; in revised form August 8, 2001; accepted August 22, 2001

The compound $Be_{1.09}B_3$ was prepared by arc-melting of the elemental constituents. The structure of single crystals taken from the arc-melted botton was determined from single-crystal X-ray data ($T = 120$ K) and is hexagonal, having space group *P6/mmm*, and lattice parameters $a = 9.7738(7)$ Å and $c = 9.5467(6)$ Å, $R = 0.047$. The structure consists of a hexagonal array of boron icosahedra, nonicosahedral B_{12} cages, and B_{18} cages. Stacked hexagonal layers of boron atoms, hexagons formed by B and Be, and equilateral triangles of boron atoms disordered by a 60° rotation exist along a 6-fold axis down the [001] direction. A superconducting transition at 0.72 K is clearly indicated by resistivity measurements.

Key Words: **superconductivity; borides; crystal structure; resistivity.**

INTRODUCTION

Since the recent discovery of superconductivity in MgB_2 at the relatively high transition temperature of 39 K (1), there has been a renewed interest in the electronic properties of intermetallic diborides belonging to the AlB_2 structure type. In particular, there have been recent attempts to substitute small Z cations in place of Mg in the hopes of achieving a higher superconducting transition temperature in the AlB_2 structure type. Beryllium is an obvious substitute choice in that it lies directly above Mg in the periodic table. Standard BCS theory (2) of superconductivity predicts enhanced transition temperatures for materials containing lighter elements due to the typically higher phonon frequencies. Given that the atomic mass ratio of Mg to Be is 2.7, one might expect to increase the superconducting transition temperature in MgB_2 by replacing Mg with Be. BeB_2 was assumed to exist as isostructural with MgB_2 and has recently been reported not to be superconducting above 5 K (3). In our efforts to synthesize BeB_2, single crystals of $Be_{1.09}B_3$ having a similar but far more complicated structure were obtained. We have found this phase to be superconducting below 0.72 K (4).

In the beryllium–boron system, several compounds have been reported including Be_6B, Be_2B, BeB_2, BeB_6 (5, 6), and BeB_3 (7). Although X-ray powder diffraction patterns of the beryllium–boron phases have been reported, detailed structural parameters have not been reported for Be_6B nor Be_2B due to the unavailability of single crystals. Single crystals of BeB_6 have been examined and found to be tetragonal (5), with lattice parameters nearly identical to those of α-AlB_{12} ($a = 10.16$ Å, $c = 14.28$ Å) (8). Oscillation and Weissenberg photographs of BeB_2 single crystals have allowed the determination of lattice parameters and Laue symmetry in the hexagonal space group, *P6/mmm* ($a = 9.79(2)$ Å, $c = 9.55(2)$ Å) (5). Here, we report the synthesis, crystal structure, and superconducting properties of $Be_{1.09}B_3$, a new binary boride, which is not likely the correct identification of the previously reported BeB_2 (5, 6) and BeB_3 phases (7, 9).

EXPERIMENTAL

Synthesis. The samples were prepared by arc-melting of the elements to prevent the incorporation of Al into the structure. Be plates (Alfa, 99.8%) and B pieces (Alfa, 99.5%) were melted together on a water-cooled copper hearth under ultra-high-purity argon gas. The starting ratio of Be to B was 4:1. Approximately 5% of the Be mass was lost during the melting process due to volatilization. Small plate-like single crystals, which were dull silver in reflected light, formed near the top of the botton. These were mechanically extracted, and single-crystal X-ray diffraction determined

---

[1] To whom correspondence should be addressed. E-mail: Julia.Chan@chem.lsu.edu. Fax: (225) 578-3458.

0022-4596/02 $35.00

the stoichiometry of the crystals to $Be_{1.09}B_3$. The remainder of the botton was copper in color, and powder X-ray diffraction determined this polycrystalline material to be Be_4B. Transport measurements were carried out on bars cut from polycrystalline samples that were arc-melted at the $Be_{1.09}B_3$ stoichiometry with an excess of 5% Be. These samples were also characterized by X-ray powder diffraction and found to have the same structure and lattice parameters identical to those of the $Be_{1.09}B_3$ single crystals.

X-Ray Powder Diffraction. X-ray powder diffraction data were obtained using a Bruker Advance D8 powder diffractometer equipped with a focusing Ge(111) incident beam monochromator ($CuK\alpha_1$ radiation). Finely ground samples were placed on a zero-background quartz sample holder. Intensity data were collected at ambient temperature in the 2θ range between 5° and 80° with a step width of 0.02° and a 2-s count time. Structural refinements have been performed with TOPAS software by Bruker AXS (10) using the structural data obtained from the single-crystal structural refinement.

Single-Crystal X-Ray Diffraction. A plate-shaped single crystal (dimensions $0.20 \times 0.18 \times 0.03\,mm^3$) was mounted on a Nonius KappaCCD diffractometer ($MoK\alpha$, $\lambda = 0.71073$ Å) and positioned under a cold stream of N_2 (120 K). Data collection parameters and crystallographic data are provided in Table 1. Intensity data were collected to a maximum θ value of 32.0°. The structure was solved by direct methods with SIR97 (11). Refinement with

TABLE 1
Crystal and Structure Analysis Data for $Be_{1.09}B_3$

Asymmetric unit	$Be_{1.09}B_3$
Z	27
Crystal dimension (mm^3)	$0.20 \times 0.18 \times 0.03$ plate, dark red
Crystal system	Hexagonal
Space group	$P6/mmm$
Lattice parameters (Å)	$a = 9.7738(7)$
$T = 120\,K$	$c = 9.5467(6)$
Cell volume (Å)	789.79(9)
ρ ($g\ cm^{-3}$)	2.400
Data Collection	
θ (°)	2.5–32.0
μ (mm^{-1})	0.082
Measured reflections	4579
Independent reflections	606
Reflections with $I > 2\sigma(I)$	484
h	−14 −> 14
k	−7 −> 6
l	−13 −> 14
R_{int}	0.028
Refinement	
$R[F^2 > 2\sigma(F^2)]$	0.047
$wR(F^2)$	0.138
S	1.124
606 reflections	
66 parameters	
$\Delta\rho_{max}$ ($e\ Å^{-3}$)	0.35
$\Delta\rho_{min}$ ($e\ Å^{-3}$)	−0.24

TABLE 2
Fractional Atomic Coordinates and Equivalent Isotropic Displacement Parameters ($Å^2$), $U_{eq} = (1/3)\sum_i \sum_j U_{ij} a^i a^j \mathbf{a}_i \times \mathbf{a}_j$

Atom	Site	Occupancy	x	y	z	U_{eq} ($Å^2$)
B1	$12p$	1	0.1640(2)	0.4926(2)	0	0.0062(4)
B2	$12n$	1	0.3480(2)	0	0.0953(2)	0.0067(4)
B3	$12o$	1	0.4470(1)	$-x$	0.1530(2)	0.0066(4)
B4	$12n$	1	0.1884(2)	0	0.1880(2)	0.0064(4)
B5	$12o$	1	0.3950(1)	$-x$	0.3071(2)	0.0069(4)
B6	$12o$	1	0.2285(1)	$-x$	0.4046(2)	0.0073(4)
B7	$6m$	0.50	0.0619(3)	$-x$	$\frac{1}{2}$	0.0062(9)
B8/Be8	$12o$	0.50/0.50	0.1191(1)	$-x$	0.3582(3)	0.0170(5)
Be9	$6m$	1	0.4395(2)	$-x$	$\frac{1}{2}$	0.0082(6)
Be10	$12n$	1	0.3644(2)	0	0.3213(2)	0.0119(5)
Be11	$2e$	1	0	0	0.1067(6)	0.010(1)
Be12	$6l$	0.50	0.1244(4)	$-x$	0	0.0131(1)
Be13	$4h$	0.125	$\frac{1}{3}$	$\frac{2}{3}$	0.125(3)	0.008(5)

TABLE 3
Selected Bond Distances

Distances (Å) within the B_{12} icosahedron	
B1–B1 (2×)	1.747(4)
B1–B2 (8×)	1.769(2)
B1–B3 (8×)	1.772(2)
B2–B2 (2×)	1.819(3)
B2–B3 (8×)	1.820(2)
B3–B3 (2×)	1.793(4)
Distances (Å) within the B_{12} and B_{18} Cages	
B5–B5 (6×)	1.808(3)
B5–B6 (12×)	1.804(2)
B6–B6 (3×)	1.821(3)
B1–B3 (12×)	1.772(2)
B3–B5 (6×)	1.715(2)
Be13–B1 (6×)	2.06(2)
Be13–B3 (3×)	1.943(4)
Be13–B5 (3×)	2.02(2)
Distances (Å) within the Be_6B_{21} Cage	
B4–B4 (6×)	1.841(2)
B4–Be8 (6×)	1.914(2)
B4–B8 (6×)	1.914(2)
B7–B8 (6×)	1.664(4)
B7–Be8 (6×)	1.664(4)
B7–B7 (6×)	1.814(9)
B7–B7 (6×)	1.047(5)[a]
B4–Be12 (24×)	2.891(2)
Be12–Be12 (6×)	2.105(7)

[a] The B7–B7 distance is between two half-populated sites.

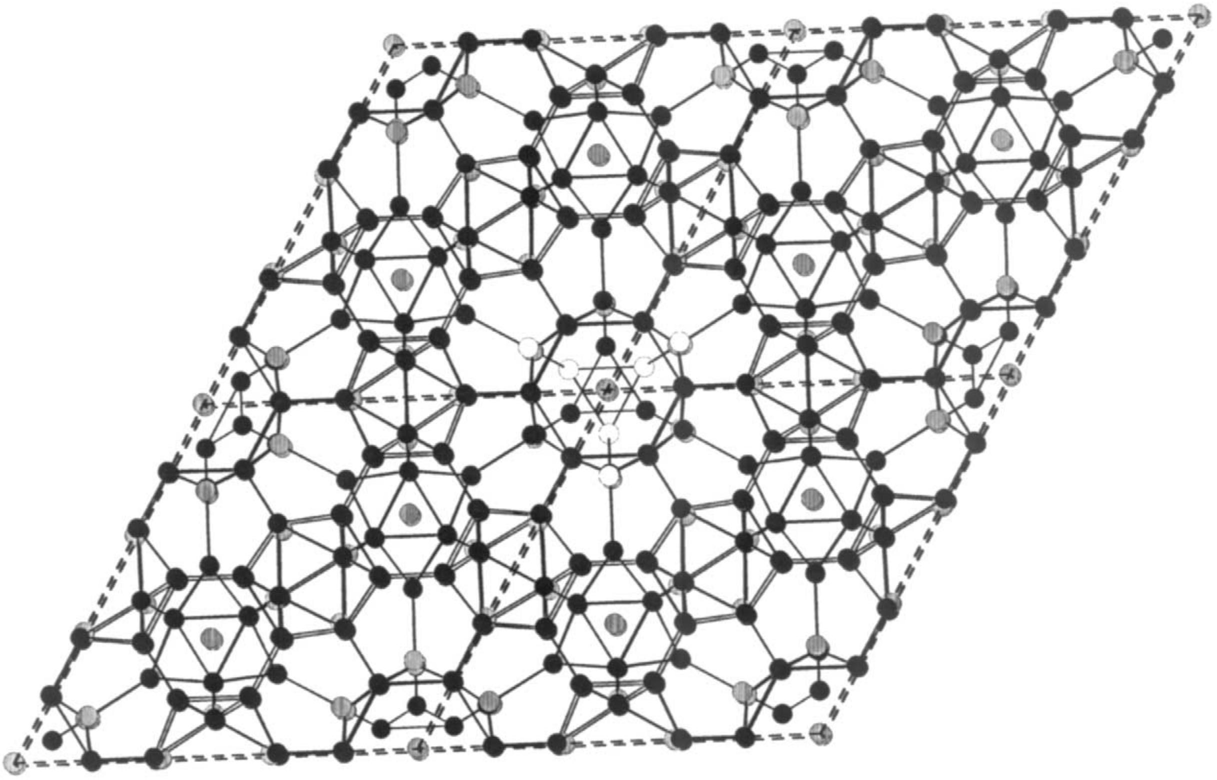

FIG. 1. Crystal structure of $Be_{1.09}B_3$ shown down the [001] axis. The gray and black circles represent Be and B, respectively. The white circles in the triangle represent one orientation of the disordered unit.

606 unique reflections yielded $R = 0.047$. The atomic coordinates are reported in Table 2. Assignment of boron or beryllium in ambiguous sites was made by examination of bond distances and displacement parameters during refinement of models with alternate assignments. B7 was assigned as half-populated on the basis of electron density and the short contacts (1.047(5) Å) to their six-fold rotated equivalents. B8/Be8 was assigned as a single site equally occupied by both atom types on the basis of packing considerations and electron density intermediate between B and Be. Occupancies of Be12 and Be13 were estimated by refinement of the multiplicities and fixed in the final refinement. Atomic coordinates and isotropic thermal parameters are provided in Table 2.

Resistivity. The resistivity of several polycrystalline samples of $Be_{1.09}B_3$ was measured between 0.05 K and 400 K using four-lead AC resistance techniques and standard lock-in detection at 1 kHz. Low-resistance electrical contacts were made to rectangular-shaped samples using silver epoxy and thin gold wires. Low-temperature magnetotransport data were collected on samples cooled in an Oxford Kelvinox dilution refrigerator to 50 mK and in magnetic fields up to 6 T. Data from 1.8 K to 300 K were collected in a Quantum Design gas flow cryostat.

RESULTS AND DISCUSSION

Crystal structure investigations were performed on powder and single crystals by X-ray diffraction. Crystallographic and data collection parameters for $Be_{1.09}B_3$ are shown in Table 1. Positional parameters with equivalent isotropic thermal parameters are provided in Table 2. Selected bond lengths and angles are given in Table 3.

We found $Be_{1.09}B_3$ to be essentially isomorphous with the previously reported BeB_3 phase. The room temperature lattice parameters from our powder diffraction refinement are $a = 9.784(3)$, $c = 9.554(2)$ Å, giving a unit cell volume of $V = 792.2(1)$ Å. The refinement of the structure with the powder data demonstrates that the polycrystalline samples have the same structure and stoichiometry as the single crystals. The previously reported BeB_3 phase was found to contain Al with stoichiometry $Al_{0.06}BeB_{3.05}$, as determined from the single-crystal study (7). Its unit cell dimensions are reported as $a = 9.800(1)$, $c = 9.535$ Å, with $Z = 26.6$. That structure differs from our results in details of the population of minor sites by beryllium and aluminum, and given the similarity in structure and lattice parameters, most likely represents an Al-doped version of $Be_{1.09}B_3$.

Similar to $Al_{0.06}BeB_{3.05}$ (7, 9) and the recently discovered scandium borocarbide $ScB_{17}C_{0.25}$ (12), $Be_{1.09}B_3$ is

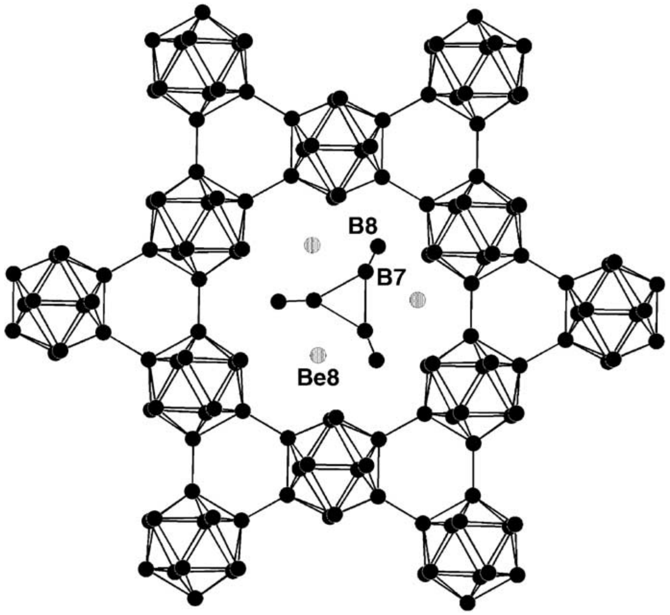

FIG. 2. Framework of the structure composed of vertex-linked sharing icosahedra and alternating B_{12} and B_{18} cages (3-fold axis). At the 6-fold axis, one orientation of the 60° disordered triangular unit is shown.

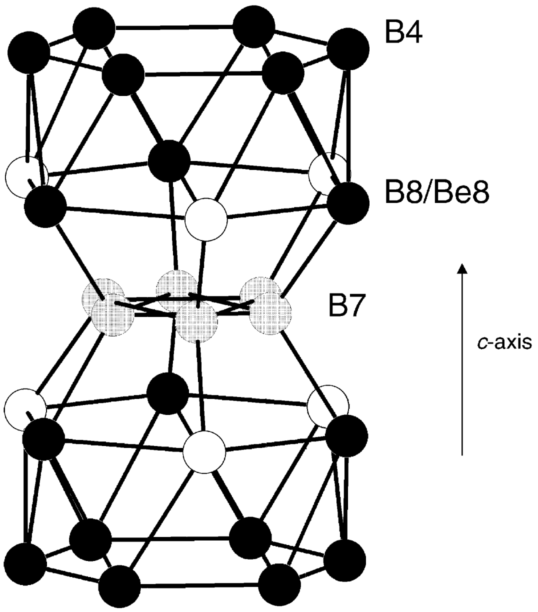

FIG. 4. Be_6B_{21} cage shown along the c-axis. The disordered triangular units are shown in gray. The adjacent layers are composed of alternating Be8 and B8 atoms.

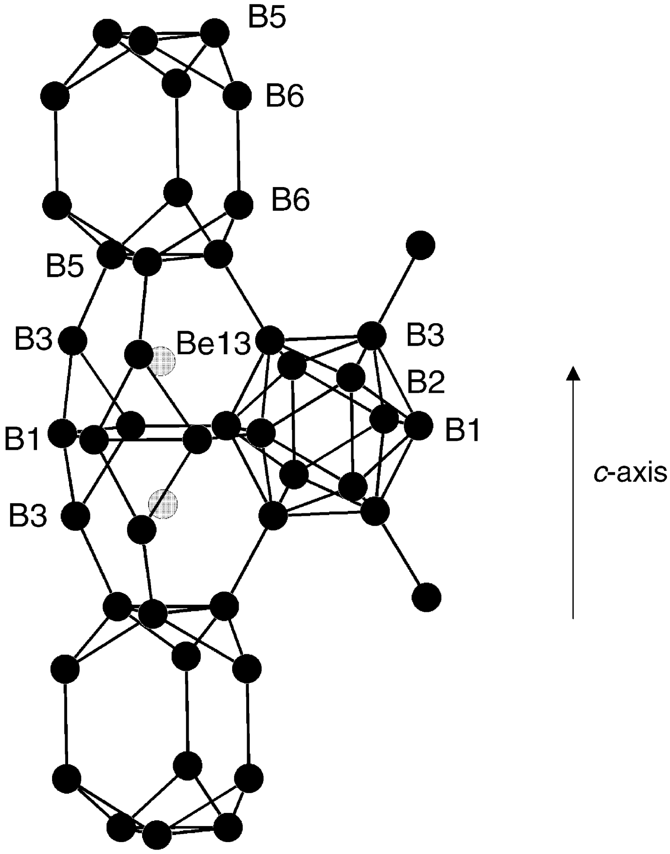

FIG. 3. View down the alternating B_{12} and B_{18} cage. Note the two Be13 atoms are partially occupied ($\frac{1}{8}$) in the B_{18} cage composed of B1, B3, and B5 atoms.

hexagonal and highly complex. The full $Be_{1.09}B_3$ structure, projected down the [001] direction, is shown in Fig. 1. The structure can be thought of as built up on a network of vertex-linked icosahedra. Figure 2 shows this hexagonal network of B_{12} icosahedra in $Be_{1.09}B_3$, viewed down the c-axis. The observed B–B distances of 1.7715(18) to 1.820(2) Å that make up the icosahedron are within the usual range found for tetragonal boron, i.e., bond distances of 1.741 to 1.873 Å (1.804 Å, average) (13), and are similar to the distances reported for $Al_{0.06}BeB_{3.05}$. As can be seen in Figs. 1–4, the structure has the following features. Three icosahedra have face-sharing contacts with a B_{18} cage, which lies on a 3-fold axis. Each icosahedron shares two adjacent triangular faces with the cage as shown in Fig. 3. Two Be13 atoms reside within the B_{18} polyhedra, each with approximately $\frac{1}{8}$ occupancy. Stacked along the c-axis sharing a triangular face with the B_{18} cage are the B_{12} nonicosahedral cages composed of B5 and B6. The location of these cages is indicated by open hexagons in Fig. 2. The observed bond distances are provided in Table 2.

Somewhat similar to the newly discovered layered superconducting MgB_2, layers of hexagons down the c-axis located at the origin are also are found in $Be_{1.09}B_3$, as shown in Fig. 4. However, the layering is more complex than in MgB_2, as equilateral triangles formed by B7 are present and are disordered around a 6-fold axis. Figure 4 shows the stacked cage-like structure (Be_6B_{21}) composed of B4 hexagons, hexagons of sites shared by B8 and

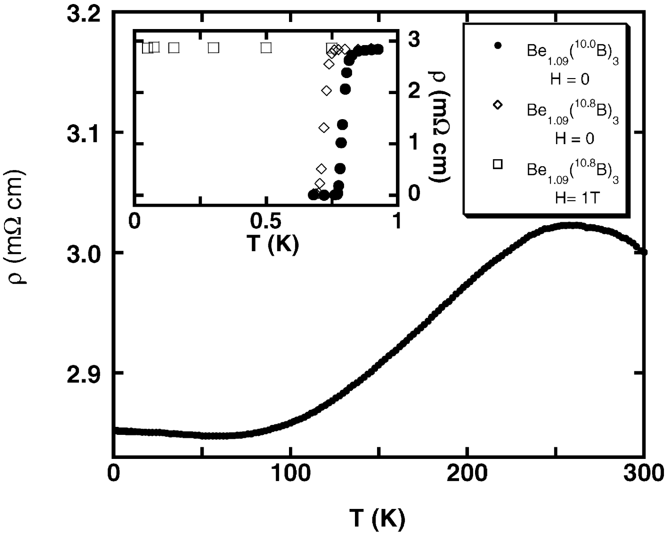

FIG. 5. Temperature-dependent resistivity of a polycrystalline sample of $Be_{1.09}B_3$. The inset shows the low-temperature superconducting transition for both $Be_{1.09}(^{10.81}B)_3$ and $Be_{1.09}(^{10}B)_3$ demonstrating a standard BCS isotope effect.

Be8 atoms, as well as the disordered B7 triangular unit. Alternating with these cages along the *c*-axis are planar hexagons of half-populated Be12 sites with an interplanar distance of 1.795 Å from a B4 hexagon. The edge of this hexagon has a Be12–Be12 distance of 2.105(7) Å.

In the interest of calculating band structure, we note that the 60° disorder exists throughout the extended structure. Only one configuration can exist per unit cell, and hence the space group for calculating the electronic properties is lowered to $P\bar{6}2m$. Calculation of the band structure is currently in progress (14).

Figure 5 displays the resistivity (ρ) from 2 to 300 K of a typical polycrystalline sample showing a weakly metallic temperature dependence characterized by a residual resistivity ratio of 1.05. The figure also displays a shallow minimum in the resistivity at 60 K followed by a maximum at 260 K. The upturn of the resistivity at low temperatures is not accompanied by any significant magnetoresistance ($\Delta\rho/\rho < 1.5e^{-4}$) and thus is not associated with quantum effects of diffusive transport or Kondo-like impurities. This unusual temperature-dependent ρ without any magnetic field sensitivity is perhaps due to scattering from nearly degenerate two-level systems associated with the inherent disorder in the crystal structure.

The low-temperature magnetotransport data of $Be_{1.09}B_3$ are shown in the inset of Fig. 5 for two samples, one made with boron in its natural abundance ($^{10.81}B$) and one from isotopically pure ^{10}B. The data clearly show a zero-field superconducting transition at 0.72 K and 0.79 K for the $^{10.81}B$ sample and the ^{10}B sample, respectively. The slight enhancement of T_c in the ^{10}B sample is qualitatively consistent with a standard BCS isotope effect. The open squares, showing the data taken in a field of 1 T, which is above the upper critical field $H_{c2} = 0.18$ T, reveal a nearly temperature-independent normal state resistivity.

In summary, the structure and resistivity of a new intermetallic superconductor $Be_{1.09}B_3$ are reported. The single-crystal X-ray data have been refined, and the compound is found to be similar to the newly discovered superconductor MgB_2, in that it contains layered B hexagons. It is the phonons associated with these hexagonal B units that are thought to be essential in producing the surprisingly high critical temperature in MgB_2. However, we find that $Be_{1.09}B_3$, which is perhaps the Be boride most closely related to MgB_2, has not only a slightly different stoichiometry, but also a much more complex and disordered structure. It is not clear at this time if the boron hexagonal units are involved in producing superconductivity in $Be_{1.09}B_3$. For this reason, and perhaps to suggest chemical substitution investigations to increase T_c, electronic structure calculations of this crystallographically complex material are of great interest.

ACKNOWLEDGMENTS

The purchase of the single-crystal X-ray diffractometer was made possible by Grant No. LEQSF (1999–2000)-ESH-TR-13, administered by the Louisiana Board of Regents. J. F. D. acknowledges support from the National Science Foundation through Grant No. DMR-9702690 and PWA acknowledges support from DMR 99-72151.

REFERENCES

1. J. Nagamatsu, N. Nakagawa, T. Muranaka, Y. Zenitani, and J. Akimitsu, *Nature* **410,** 63 (2001).
2. M. Tinkam, "Introduction to Superconductivity." McGraw-Hill, New York, 1996.
3. I. Felner, http://xxx.lanl.gov/cond-mat/0102508 (2001).
4. D. P. Young, D. Browne, P. Adams, J. Y. Chan, and F. R. Fronczek, http://xxx.lanl.gov/abs/cond-mat/0104063 (submitted).
5. D. E. Sands, C. F. Cline, A. Zalkin, and C. Hoenic, *Acta Crystallogr.* **14,** 309 (1961).
6. C. L. Hoenig, C. F. Cline, and D. E. Sands, *J. Amer. Ceram. Soc.* **44,** 385 (1961).
7. V. R. Mattes, K. F. Tebbe, H. Neidhard, and H. Rethfeld, *Z. Anorg. Allg. Chem.* **413,** 1 (1975).
8. I. Higashi, *J. Solid State Chem.* **154,** 168 (2000).
9. R. Mattes, K. F. Tebbe, H. Neidhard, and H. Rethfeld, *J. Less-Common Met.* **47,** 29 (1976).
10. TOPAS — General profile and structure analysis software for powder diffraction data, Bruker AXS 2.0, 2000.
11. A. Altomare, G. Cascarano, C. Giacovazzo, A. Guagliardi, M. C. Burla, G. Polidori, and M. Camalli, *J. Appl. Cryst.* **27,** 435 (1994).
12. T. Tanaka, *J. Alloys Compd.* **270,** 132 (1998).
13. J. L. Hoard, R. E. Hughes, and D. E. Sands, *J. Am. Chem. Soc.* **80,** 4507 (1958).
14. D. A. Browne and R. L. Kurtz, to be published.